HEFAT2014
10th International Conference on Heat Transfer, Fluid Mechanics and Thermodynamics
14 – 16 July 2014
Orlando, Florida

Lagrangian Block Simulation of Buoyancy At Turbulence Interfaces

Chu, Vincent H.* and Altai, Wihel
*Author for correspondence
Department of Civil Engineering and Applied Mechanics,
McGill University,
Montreal, Quebec H3A 2K6,
Canada,
E-mail: vincent.chu@mcgill.ca

ABSTRACT

Simulations of turbulent interfaces produced by positive and negative buoyancy are conducted by moving blocks of fluid in the direction of the flow. The second moment of the blocks increases at a rate proportional to the diffusivity. The block simulation is free of numerical oscillations. Unlike most classical methods, the error associated with Lagrangian block simulation is not cumulative. Artificial diffusion error is negligible. The non-diffusive Lagrangian block simulations have provided reliable data to evaluate the performance of (i) sub-grid scale modelling and (ii) K-ε modelling of turbulent flow under the opposing influence of buoyancy.

INTRODUCTION

Most computational fluid-dynamics codes are developed using the Eulerian description. To find the numerical solution, fluxes are estimated on the surface of the finite volume using a truncation series. Spurious numerical oscillations and artificial numerical diffusion are consequences, particularly in regions across flow discontinuities. Diffusion often is introduced synthetically in many schemes to gain computational stability. Occasional switching to a diffusive upwind scheme is one classic strategy to manage the numerical oscillations [1,2,3,4,5]. Lagrangian block simulation (LBS) offers an alternative that could eliminate the spurious numerical oscillations and false diffusive error [6,7]. The blocks move in the direction of the flow. The squares of the block widths expand in proportion to the diffusivities. The block simulation procedure consists of three steps: (i) Lagrangian advection and diffusion, (ii) division into portions, and (iii) reassembly of the portions into new blocks. The blocks are renewed in each time increment to prevent excessive distortion. In this paper simulation of buoyancy at turbulence interfaces has been carried out using the LBS method. In one series of simulations, the Kelvin-Helmholtz instabilities initiate turbulence across stably stratified interface. In the other series of simulations, the Rayleigh-Taylor instabilities due to negative buoyancy initiate the interface. Across the stably stratified interface, the velocity difference is the source of turbulence production. The turbulent motion is bounded by the stable stratification. In the unstably stratified flow, turbulent motion is initiated by negative buoyancy. The subsequent development across the unstable interface is unbounded, as the turbulence is produced continuously by the positive work done by buoyancy force.

The simulation data derived from the two series of simulations are employed to evaluate (i) the role of sub-grid modelling in LES, and (ii) the empirical modification to K-e modelling of the turbulent flows under opposing buoyancy influences.

NOMENCLATURE

Cp_x	Convergence coefficients, *x*-component
Cp_y	Convergence coefficients, *y*-component
D_x, D_y	Diffusion coefficient components in *x*-*y* directions
G	Mean buoyancy per unit mass
g'	$= g\Delta\rho/\rho$ = reduced gravity = buoyancy per unit mass
LBS	Lagrangian Block Simulation
m_p	Mass of the portions
m	Block mass
p	pressure
U	Mean velocity in the longitudinal direction
u, v	*x*-*y* components of the velocity
x_c, y_c	*x*-*y* coordinates of the mass centre of the block
z	Coordinate downward from the top of the inversed layer
$\bar{z}$	Elevation of the mass centre downward from the top of the inversed layer

Special characters

Δt	Time step size
$\Delta x, \Delta y$	Grid size
σ	Thickness of the mixing region in top-heavy exchange
σ_x, σ_y	Second moments in *x*-*y* directions
$\sigma_K, \sigma_\varepsilon$	Adjustable constants of the standard K-ε model
w_x, w_y	Block widths in *x*-*y* directions
ψ	Stream function

ζ	z-component of vorticity

Subscripts and Superscripts

n	Time step
n_p	Total number of portions
p	p = 1 to 9 is the index identifying the portion
i, j	Index identifying the cell

LAGRANGIAN BLOCK ADVECTION

The Lagrangian blocks are containers of mass and momentum that are transported and diffused in the direction of the flow. In two dimensions, a block is defined by its centre of mass (x_c, y_c) and widths (w_x, w_y) as shown in Figure 1.

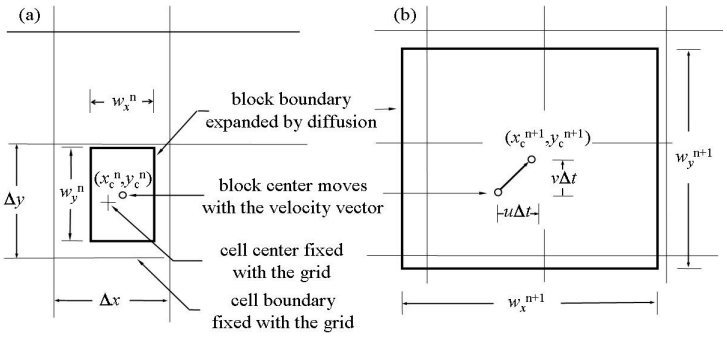

Figure 1 Lagrangian block advection and diffusion. (a) The initial block position (x_c^n, y_c^n) and dimensions (w_x^n, w_y^n) before the advection and diffusion at time $t = t^n$. (b) The displaced-and-deformed block position (x_c^{n+1}, y_c^{n+1}) and dimensions (w_x^{n+1}, w_y^{n+1}) after the advection and diffusion at time $t = t^{n+1}$

Over a period of one time step, Δt, the displacements of the block's mass centre in x- and y-directions are time integration of velocity from time $t = n\Delta t$ to $t = (n+1)\Delta t$:

$$x_c^{n+1} = x_c^n + \int_{n\Delta t}^{(n+1)\Delta t} u(x_c, y_c)\,dt \tag{1}$$

$$y_c^{n+1} = y_c^n + \int_{n\Delta t}^{(n+1)\Delta t} v(x_c, y_c)\,dt \tag{2}$$

LAGRANGIAN LAW OF DIFFUSION

The diffusion is simulated by continuous increase of the block widths (w_x, w_y) with time. The exchange of contents in the overlapping region between the neighbouring blocks can produce the diffusion. In his study of Brownian motion, Einstein [8] has shown that the second moments (σ_x^2, σ_y^2) of the random walk increase at a rate in proportion to the diffusion coefficients (D_x, D_y):

$$D_x = \frac{1}{2}\frac{d\sigma_x^2}{dt}, \quad D_y = \frac{1}{2}\frac{d\sigma_y^2}{dt} \tag{3}$$

Since the second moments (σ_x^2, σ_y^2) of rectangular blocks are

$$\sigma_x^2 = \frac{1}{12}w_x^2, \quad \sigma_y^2 = \frac{1}{12}w_y^2, \tag{4}$$

the width squares (w_x^2, w_y^2) are assumed to increase at a rate in proportion to diffusion coefficients, according to the *Lagrangian law of block diffusion*:

$$D_x = \frac{1}{24}\frac{dw_x^2}{dt}, \quad D_y = \frac{1}{24}\frac{dw_y^2}{dt} \tag{5}$$

Figure 1 defines the widths of the block (w_x, w_y) before and after the advection-and-diffusion step. The integration of the law of block diffusion over one time increment gives the following formula for the widths of the block after one Lagrangian diffusion step

$$w_x^{n+1} = \sqrt{(w_x^n)^2 + 24\int_{n\Delta t}^{(n+1)\Delta t} D_x(x_c, y_c)\,dt} \tag{6}$$

$$w_y^{n+1} = \sqrt{(w_y^n)^2 + 24\int_{n\Delta t}^{(n+1)\Delta t} D_y(x_c, y_c)\,dt} \tag{7}$$

Equations. 1, 2, 6 and 7 are the incremental equations used to calculate the displacement and deformation of the blocks over one Lagrangian advection-and-diffusion step.

DIVISION INTO PORTIONS AND REASSEMBLY INTO NEW BLOCKS

To prevent excessive deformation during the Lagrangian advection, the blocks are subdivided along the grid lines and then reassembled into new blocks in every time increment after the advection-and-diffusion step. The procedures used to divide the blocks into portions which are then reassembled into the new blocks are described in Figure 1b and Figure 2.

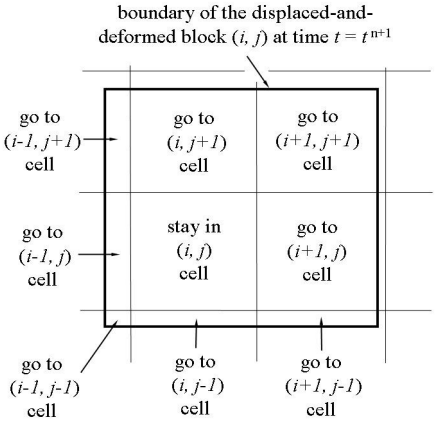

Figure 2 Division of a block along the grid lines into portions after the Lagrangian advection-and-diffusion step.

As many as nine portions can be produced from one (i, j) block. One of the portions stays in the (i, j) cell. The other goes to the neighbouring cells. The number of portions in a cell is n_p, varying from zero to nine. New blocks are constructed from the portions in each cell by the conservation of the moments in the cell.

Equating the zero moment of the new block to the sum of the zero moments of all portions in the cell,

$$m = \sum_{p=1}^{n_p} m_p \tag{8}$$

where m = total mass of the new block and m_p = mass of a portions. The index p identifies the portion. Equating the first moment,

$$m x_c = \sum_{p=1}^{n_p} m_p x_{cp} \tag{9}$$

$$m y_c = \sum_{p=1}^{n_p} m_p y_{cp} \tag{10}$$

Equating the second moments,

$$m\left(x_c^{\,2} + \frac{1}{12} w_x^{\,2}\right) = \sum_{p=1}^{n_p} m_p \left(x_{cp}^{\,2} + \frac{1}{12} w_{xp}^{\,2}\right) \tag{11}$$

$$m\left(y_c^{\,2} + \frac{1}{12} w_y^{\,2}\right) = \sum_{p=1}^{n_p} m_p \left(y_{cp}^{\,2} + \frac{1}{12} w_{yp}^{\,2}\right) \tag{12}$$

The centre of mass of the new block is determined by Eqs. 9 and 10:

$$x_c = \frac{1}{m} \sum_{p=1}^{n_p} m_p x_{cp} \tag{13}$$

$$y_c = \frac{1}{m} \sum_{p=1}^{n_p} m_p y_{cp} \tag{14}$$

The widths of the new block are determined by Eqs. 11 and 12:

$$w_x = \sqrt{\frac{1}{m} \sum_{p=1}^{n_p} m_p \left(12 x_{cp}^{\,2} + w_{xp}^{\,2}\right) - 12 x_c^{\,2}} \tag{15}$$

$$w_y = \sqrt{\frac{1}{m} \sum_{p=1}^{n_p} m_p \left(12 y_{cp}^{\,2} + w_{yp}^{\,2}\right) - 12 y_c^{\,2}} \tag{16}$$

The computational algorithm used in the construction of the new blocks at each time increment is centred around the (*i, j*) cell. The algorithm first subdivides the block along the grid lines to find the portion that stays in the (*i, j*) cell and the portions that go to its neighbouring blocks. The portions are then used in the construction of the new block by conserving the moments.

CONVERGENCE PARAMETER

Figure 3 shows the blocks after the advection-and-diffusion step, the subdivision of the blocks into portions and the assembly of the portions to form new blocks in the simulation of a starting jet. The computer algorithm has been developed on the assumption that the block boundaries at the end of the advection-and-diffusion step stay within the immediate neighbouring cells. This assumption leads to the necessary condition for convergence of the numerical solutions. The displacement of the block boundary on one side of the block by diffusion plus advection must not exceed the size of one cell. This leads us to the necessary conditions that

$$\frac{1}{2}\left(w_x^{\,n+1} - w_x^{\,n}\right) + |u|\,\Delta t < \Delta x \tag{17}$$

$$\frac{1}{2}\left(w_y^{\,n+1} - w_y^{\,n}\right) + |v|\,\Delta t < \Delta y \tag{18}$$

Using Eqs. 6 and 7 to find $w_x^{\,n+1}$ and $w_y^{\,n+1}$, and letting $w_x^{\,n} = \Delta x$ and $w_y^{\,n} = \Delta y$, these necessary conditions then become

$$\mathrm{Cp}_x = \sqrt{\frac{1}{4} + 6\frac{D_x \Delta t}{(\Delta x)^2}} - \frac{1}{2} + \frac{|u|\,\Delta t}{\Delta x} < 1 \tag{19}$$

$$\mathrm{Cp}_y = \sqrt{\frac{1}{4} + 6\frac{D_y \Delta t}{(\Delta y)^2}} - \frac{1}{2} + \frac{|u|\,\Delta t}{\Delta y} < 1 \tag{20}$$

For convergence of the block simulations, the time step Δt must be selected to limit the convergent parameters Cp_x and Cp_y in the x- and y-directions to values less than unity.

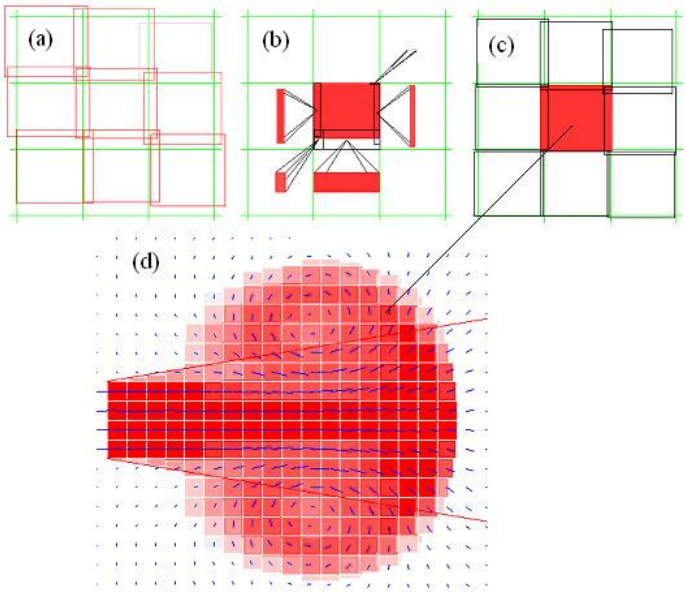

Figure 3 (*a*) The block (i, j) and its neighbours after the Lagrangian advection-and-diffusion step. (*b*) The portions within the (i, j) cell. (*c*) New (i, j) block obtained from the reassembly. (d) All of the blocks and the velocity vectors in the simulation of a starting jet.

BUOYANCY EFFECT ON TURBULENCE

The model simulation for buoyancy effect on turbulence is two-dimensional. Calculations for the flow are based on the stream function and vorticity formulation. The stream function ψ is defined by the velocity (*u, v*):

$$u = +\frac{\partial \psi}{\partial y}, \quad v = -\frac{\partial \psi}{\partial x} \tag{21}$$

while the vorticity ζ is determined by the Poisson equation:

$$\zeta = -[\frac{\partial^2 \psi}{\partial x^2} + \frac{\partial^2 \psi}{\partial y^2}] \tag{22}$$

Buoyancy creates vorticity. The rate of vorticity creation is readily derived from on the Euler equations:

$$\frac{Du}{Dt} = -\frac{1}{\rho}\frac{\partial p}{\partial x}, \quad \frac{Dv}{Dt} = -\frac{1}{\rho}\frac{\partial p}{\partial y} + g' \tag{23}$$

in which $g' = g\ (\Delta\rho/\rho)$ is the buoyancy force per unit mass of the fluid. Following the motion of the fluid, the vorticity

$$\zeta = \frac{\partial v}{\partial x} - \frac{\partial u}{\partial y} \tag{24}$$

changes at a rate that is due to variation of buoyancy in space:

$$\frac{D\zeta}{Dt} = \frac{\partial g'}{\partial x} \tag{25}$$

Without source, the buoyancy is conserved:

$$\frac{D\,g'}{Dt} = 0 \tag{26}$$

Diffusion is not explicit in a Lagrangian formulation. The effect of the diffusion however is included in the *Lagrangian law of diffusion* (Equation 5). Equations 6 and 7 calculate the expansion of the blocks for the diffusion effect. Equations 25 and 26 determine the variations of the vorticity ζ and buoyancy g' in the blocks as the blocks move in the direction of the flow. The Fick's law of diffusion is an Eulerian concept and therefore has no part in any of the Lagrangian formulation [7][8].

LARGE EDDY SIMULATION

The Large Eddy Simulation (LES) for the turbulent flows of opposing buoyancy are conducted using a sub-grid scale model according to Smagorinsky [9]. The diffusion coefficients, D_x and D_y in Equations 6 and 7, are the Smagorinsky's sub-grid-scale viscosity:

$$D_x = D_y = \nu_{SG} = C_s^2\,\Delta^2\,\sqrt{S_{ij}S_{ij}} \tag{27}$$

where $\Delta = \sqrt{(\Delta x)^2 + (\Delta y)^2}$ and S_{ij} is the strain-rate tensor:

$$S_{ij} = \frac{\partial u_i}{\partial x_j} + \frac{\partial u_j}{\partial x_i}, \quad i = 1,2, \quad j = 1,2 \tag{28}$$

The Smagorinsky coefficient selected for the present simulations are: C_s = 0.0375, 0.075, and 0.15. The difference in diffusion between these selections is huge (16-fold) since the sub-grid viscosity is proportional to the square of the value of C_s. These diffusion coefficients however are in the range recommended by Ferziger & Peric [10].

Turbulence Interfaces

The buoyancy force in the flow of non-uniform buoyancy may do positive work to produce the turbulent motion, or may do negative work to suppress the motion. To study this body-force effect on turbulence, the numerical simulations were conducted for two turbulent flows with opposite buoyancy stratification. In one flow, turbulence was produced by the Kelvin-Helmholtz (KH) instabilities due to velocity difference across a stably stratified interface (Figure 1). In the other flow, turbulence was produced by the Rayleigh-Taylor (RT) instabilities due to buoyancy force across an unstably stratified interface (Figure 2). For the stably stratified flow, the velocity difference across the interface initiated the turbulent motion by the KH instabilities. The subsequent development of turbulent motion in the mixing region across the interface is bounded by the stabilizing effect of the buoyancy stratification. On the other hand in the unstably stratified flow, the motion was initiated by the RT instabilities. The turbulence in the inverse layer across the unstable interface is unbounded as turbulent motion is produced continuously and intensified due to the positive work done by the buoyancy force.

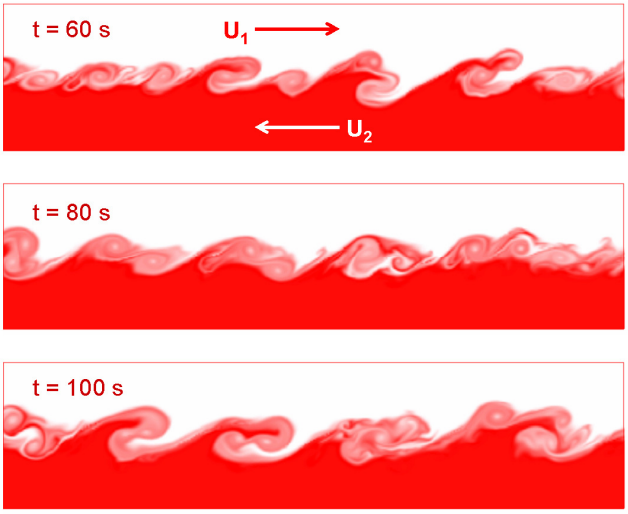

Figure 4 Turbulence initiated by Kelvin-Helmhotz instabilities across a stably stratified interface. The lighter fluid in the upper layer moves to the right while the heavier fluid in the lower layer moves in the opposite direction, to the left. LES using a sub-grid viscosity Cs =0.075.

Kelvin-Helmhotz Instability

The first series of LES are carried out for the stably stratified flow of two layers in a long and horizontal tank. The bottom layer is heavier than the top layer. The initially stagnant fluids are perturbed by tilting the long tank onto an incline for a brief period of time, as it was performed in the laboratory experiment by Thorpe [11]. A quasi-steady stably stratified flow shear flow eventually is established to produce a mean buoyancy profile $G(y)$ and mean velocity profile $U(y)$. The Richardson number

Ri associated with the quasi-steady state according to the present series of LES is

$$\mathrm{Ri} = \frac{\dfrac{\partial G}{\partial y}}{\left(\dfrac{\partial U}{\partial y}\right)^2} \cong 0.3 \qquad (29)$$

This value of the Richardson number obtained from the LES for the stably stratified flow is in close agreement with the laboratory observation by Thorpe [11].

Rayleigh-Taylor Instabilities

The second series of LES is conducted for the exchange of fluid between two layers in a tank of unstable stratification. The fluid in the tank is top-heavy in the laboratory experiment by Li and Chu [12]. Figure 5 shows the growth of the top-heavy mixing region obtained from a LES at times t = 5s, 7s and 11s. Figure 6 shows the images of the top-heavy exchanges at two subsequent times in one of the laboratory experiments by Li and Chu [12]. The arrows in the figure show the directions of the exchange fluids in the laboratory experiment. Turbulence initiated by the Rayleigh-Taylor instabilities is produced continuously as the heavy fluid from the top layer sinks, and the fluid from the bottom rises to replace the sinking fluid. The exchange of fluids across the gravitationally unstable interface is loosely describable by a plume model. The length scale of the plumes increases continuously as adjacent plumes merge to form plumes of greater size.

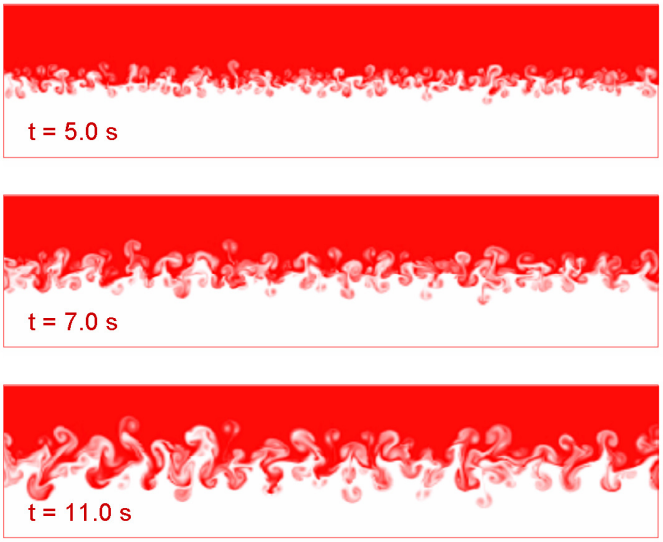

Figure 5 Turbulence produced by Rayleigh-Taylor instabilities across an unstably stratified interface obtained from a LES using a sub-grid viscosity $C_s = 0.075$

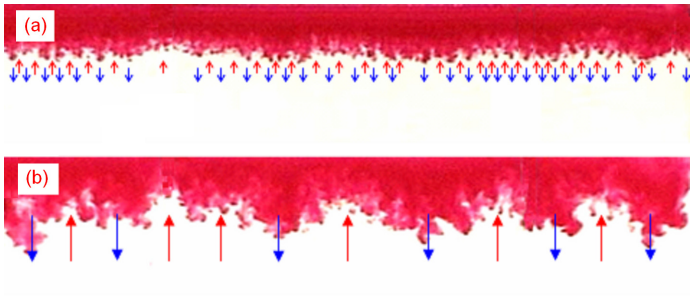

Figure 6 Images of the exchanges across the interface in the top-heavy mixing region observed at two subsequent times in a laboratory experiment [12].

Measurements were made of the mass concentration to determine the buoyancy g' during the laboratory experiments. Mean buoyancy profiles $G(y, t)$ were obtained by averaging the mass concentration obtained from the laboratory measurements and from the large-eddy simulations. The mass centre of the top-heavy mixing region is calculated from the simulation using the definition

$$\bar{y}(t) = \frac{\int y \, \mathrm{d}G}{\int \mathrm{d}G} \qquad (30)$$

The depth of the top-heavy mixing region is calculated using

$$\sigma(t) = \frac{\int (y - \bar{y})^2 \mathrm{d}G}{\int \mathrm{d}G} \qquad (31)$$

The depth of the mixing layer, $\sigma(t)$, increases without bounded as the turbulent kinetic energy in the mixing region is continuously produced by the positive work done by the buoyancy force.

LES Model of Rayleigh-Taylor Instabilities

Figure 7 presents the LES results obtained for the dimensionless depth of the mixing region, $\sigma(t)/h_1$, as a function of dimensionless time, t/t_s. The length scale h_1 is the initial depth of the top layer. The time scale is $t_s = h_1/g_o$, in which g_o is the buoyancy initially associated with the upper layer [12]. The best fit to the simulation data gives

$$\frac{\sigma}{h_1} = 0.014 \frac{t^2}{t_s^2} \qquad \text{for} \qquad t \le 7 \qquad (32)$$

$$\frac{\sigma}{h_1} = 0.125 \frac{t}{t_s} - 0.2 \qquad \text{for} \qquad t > 7 \qquad (33)$$

These formulae obtained from LES are in close agreement with the experimental data observed by Li and Chu [12].

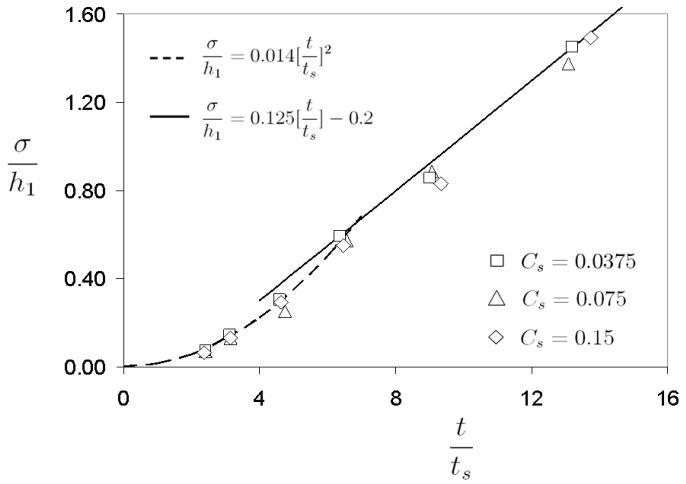

Figure 7 Depth variations with time of the top-heavy mixing obtained by LES using different levels of sub-grid viscosity.

The three Smagorinsky coefficients C_s = 0.0375, 0.75 and 0.15 used in the LES have produced almost the same mixing depth variation in time as shown in Figure 7 and similar image of the mixing region in Figure 8. The variation in sub-grid viscosity is 16-fold as the sub-grid viscosity is proportional to the square of the value of C_s. The mixing region appears to be independent of the level of the sub-grid viscosity. The overall structure of the mixing regions obtained using the very different sub-grid-scale viscosity is not significantly different.

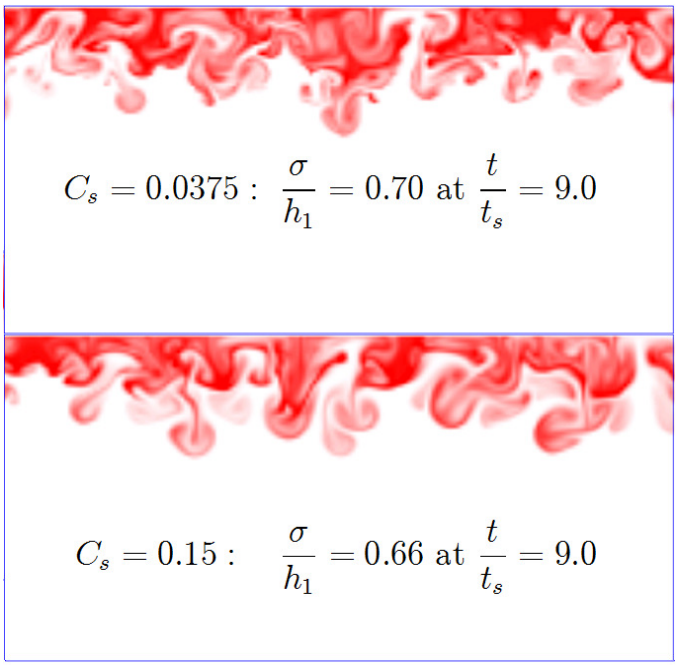

Figure 8 Results of two LES of the top-heavy mixing region produced by 16-fold increase in the sub-grid-scale viscosity corresponding to C_s = 0.0375 and 0.15.

K-ε MODELLING SIMULATION

The alternative to LES is to use the K-ε turbulence model. To include the buoyancy effect on turbulence, Gibson & Launder [13] and Hossian & Rodi [14][15] have modified the standard K-ε model. Their buoyancy-extended model equations are:

$$\frac{DK}{Dt} = \frac{\partial}{\partial x_\alpha}[\nu_K \frac{\partial K}{\partial x_\alpha}] + P - W - \varepsilon \tag{34}$$

$$\frac{D\varepsilon}{Dt} = \frac{\partial}{\partial x_\alpha}[\nu_\varepsilon \frac{\partial \varepsilon}{\partial x_\alpha}] + c_{1\varepsilon}\frac{\varepsilon}{K}[P - (1-c_{3\varepsilon})W] - c_{2\varepsilon}\frac{\varepsilon^2}{K} \tag{35}$$

in which P is the production term and W is the work done by the buoyancy force.

The buoyancy does negative work to suppress the turbulence in the simulations for the Kelvin-Helmhotz instabilities and positive work for Rayleigh-Taylor instabilities; i.e.,

$$W = -\overline{g'w'} < 0 \quad \text{for the stably stratification}$$

$$W = -\overline{g'w'} > 0 \quad \text{for the unstably stratification}$$

The turbulence also is produced by mean shear, due to the production term

$$P = -\overline{u'w'}\frac{\partial U}{\partial z}$$

The K-ε model viscosity is determined by

$$\nu_K = \frac{\nu_T}{\sigma_K}, \quad \nu_\varepsilon = \frac{\nu_T}{\sigma_\varepsilon}, \quad \nu_T = C_\mu \frac{K^2}{\varepsilon} \tag{36}$$

The values of the adjustable constants of the standard K-ε model are [16]: c_μ = 0.09, $\sigma_{1\varepsilon}$ = 1.00, $\sigma_{2\varepsilon}$ = 1.30, $c_{1\varepsilon}$ = 1.44, $c_{1\varepsilon}$ = 1.92. The additional adjustable constant in the buoyancy-extended model, $c_{3\varepsilon}$, is not universal and needs to be determined from calibration by comparing simulation results with available experimental data.

K-ε Modelling of Kelvin-Helmholtz Instabilities

Figure 9 shows the results of the K-ε modelling simulation for the Kelvin-Helmholtz instabilities obtained using two different modelling constants: $c_{3\varepsilon}$ = 0.4 and $c_{3\varepsilon}$ = 1.0. The Richardson numbers of the simulated turbulent flow in quasi-steady state are Ri = 0.64 and Ri = 0.35, respectively. Hossian & Rodi suggested $c_{3\varepsilon}$ = 1.0. However, a smaller $c_{3\varepsilon}$ = 0.9 would give a Richardson number of Ri = 0.26, which is in closer agreement with experimental observation [17]. It is clear that

successful simulations of the turbulence interface by the buoyancy-extended K-ε model are critically dependent on the value of the adjustable constant $c_{3\varepsilon}$ selected for the simulations.

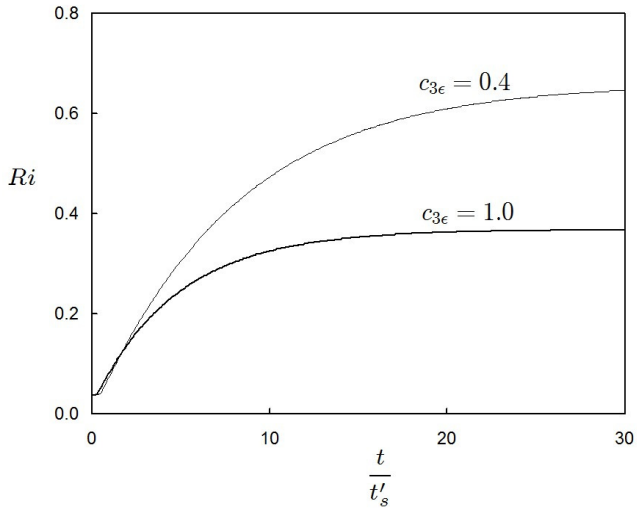

Figure 9 Richardson number Ri with dimensionless time t/t_s where $t_s = (U_1\text{-}U_2)/g_o'$ is the time scale of the Kelvin-Helmholtz instabilities. The quasi-steady value are Ri = 0.35 if $c_{3\varepsilon}$ = 1.0 and Ri = 0.63 if $c_{3\varepsilon}$ = 0.4

K-ε Modelling of Rayleigh-Taylor Instabilities

Figure 10 shows the modelling simulations for one tank-overturn experiment in the laboratory conducted by Li & Chu [12]. These simulations for Rayleigh-Taylor instabilities have led to entirely different values for the modified adjustable constant. The selection of a value of $c_{3\varepsilon}$ = 0.4 has led to best fit of the tank-overturn laboratory data obtained by Li & Chu [12]. This value however is not the value of $c_{3\varepsilon}$ = 0.9 recommended to fit the laboratory data of the Kelvin-Helmhotz instabilities. The results of the K-ε modelling simulations for the Rayleigh-Taylor instabilities are extremely sensitive to the selection of the buoyancy-extended modelling constant. A small change in the buoyancy-extended constant has produced enormously different results. The depth in the mixing region, σ, increases four-fold as the modified constant changes from $c_{3\varepsilon}$ = 0.4 to 0.6.

The recommended adjustable constant $c_{3\varepsilon}$ in the buoyancy-extended K-ε model is 0.4 for the simulation of the turbulence interface produced by the Rayleigh-Taylor instabilities. Using this same $c_{3\varepsilon}$ value of 0.4 would produce entirely unrealistic simulations of the Kelvin-Helmholtz instabilities (see Figure 9). It is unclear how the standard K-ε model can be modified for simulation of the buoyancy effect. It is also unclear how the model coefficient is to be selected for the model's dependency on the direction of buoyancy in the flow. The buoyancy-extended model of Gibson & Launder [13] and Hossian & Rodi [14][15] is not acceptable, as vastly different simulation results are produced by small change in value of the model's adjustable constant, $c_{3\varepsilon}$.

CONCLUSION

Numerical simulation of buoyancy effect on turbulence has been carried out by moving blocks of fluid in the direction of the flow using the Lagrangian block simulation method. Results of the LES modelling have produced accurate and reliable results that are not sensitive to the selection of Smagorinsky's coefficient for the sub-grid-scale viscosity. The K-ε model on the other hand does not generally give acceptable results. The buoyancy-extended modelling coefficient $c_{3\varepsilon}$ is not constant. The K-ε model simulations of Kelvin-Helmholtz instabilities in a stably gravity-stratified flow have suggested a buoyancy-extended coefficient of $c_{3\varepsilon}$ = 0.9. The simulations for the Rayleigh-Taylor instabilities on the other hand would produce acceptable results only when a very different value of $c_{3\varepsilon}$ = 0.4 is selected.

The success of the present LES for the buoyancy effect on turbulence is directly attributable to the use of the Lagrangian block simulation method, which has been shown to produce simulation results without cumulative false diffusion error [7]. The Lagrangain block simulation also has been shown to have excellent numerical computational stability in a series of simulations for different problems [7][18][19][20][21].

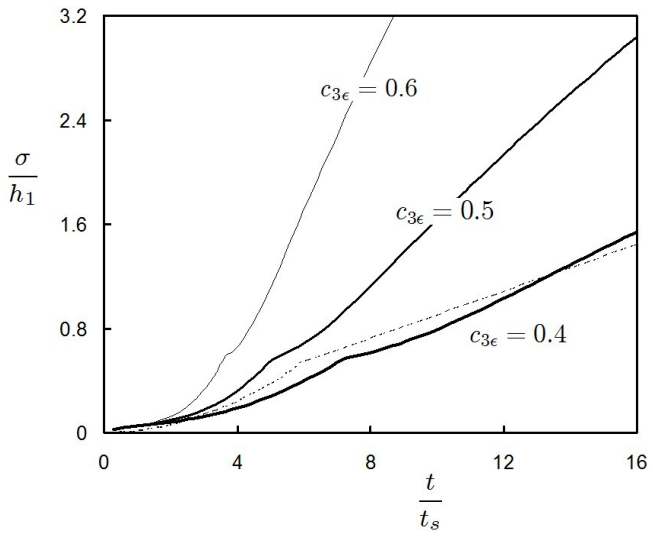

Figure 10 Depth of the top-heavy mixing region, σ, with dimensionless time, t/t_s, where $t_s = \sqrt{g'_o h_1}$ is the time scale of the Rayleigh-Taylor instabilities. Dash line shows the data of the laboratory experiment by Li & Chu [12]. The solid lines are the results of the K-ε modelling simulations obtained from three buoyancy-extended modelling constants.

REFERENCES

[1] Leonard, B.P., A stable and accurate convective modelling procedure based on quadratic upstream interpolation, *Computer Methods in Applied Mechanics and Engineering*, Vol. 19, 1979, pp 59-98.

[2] Leonard, B.P. and Mokhtari, S., Beyond first-order upwinding: the ultra-sharp alternative for non-oscillatory steady-state simulation of convection, *Int. J. Numerical Methods in Engrg*., Vol. 30, 1990, pp 729-766

[3] Lien, F.S. and Leschziner, M.A., Approximation of turbulence convection in complex flow with a TVD-MUSCL Scheme, *Proc. 5th Int. Symp. on Refined Modelling and Turbulence Measurements*, Paris, September 7-10, 1993.

[4] Pinilla, C., Bouhairie, S., Tan, L.W. and Chu, V.H., Minimal intervention to simulations using the shallow-water equation, *J. Hydro-Environ. Res*., Vol. 4, part 2, 2010, pp 201-207.

[5] Chu, V.H. and Gao, C. False diffusion produced by flux limiters, *Computational Thermal Sciences*, Vol. 5(6), 2013, pp. 503-520.

[6] Tan, L.-W. and Chu, V.H., Two-dimensional simulation of shallow-water waves by Lagrangian block advection, *Computers and Fluids*, Vol. 65, 2012. pp. 35-43.

[7] Chu, V.H. and Altai, W., Advection and diffusion simulations using Lagrangian blocks, *Computational Thermal Sciences*, Vol. 4(4), 2012, pp. 351-363.

[8] Einstein, A. (1905) This and other articles of Einstein is collected in a book entitled Investigations on the *Theory of Brownian Movement*, edited by R. Futh, translated by A. D. Cowper (Dutton, New York), *Ann. d. Physik.*, Vol. 17, 549 pp

[9] Smagorinsky, J., General circulation experiments with the primitive equations. I: the basic experiment, *Monthly Weather Review,* 1963, Vol. 91, pp 99-164.

[10] Ferziger, J.H. and Peric, M., *Computational Methods for Fluid Dynamics*, Springer, New York, 1999, 389 pp.

[11] Thorpe, S.A., Experiments on the instability of stratified shear flow: miscible fluids, *J. Fluid Mech.*, Vol. 46, 1971, pp. 299-319.

[12] Li, X. and Chu, V.H. , Turbulence and mixing across gravitationally unstable interface by tank-overturn experiment, *J. Hydro-environment Research*, Vol 1, No. 3-4, 2008, pp. 176-186.

[13] Gibson, M.M. and Launder, B.E., On the calculation of horizontal non-equilibrium turbulent flow under gravitational influence, *J. Heat Transfer*, ASME, Vol. 98(C1), 1976, pp. 81-87.

[14] Hossain, M.S. and Rodi, W., A turbulence model for buoyant flows and its application to vertical buoyant jets, in *Turbulent Buoyant Jets and Plumes*, W. Rodi ed., HMT-Series, Vol. 6, Pergamon Press, Oxford, England, 1982.

[15] Hossain, M.S. and Rodi, W., Mathematical modelling of vertical mixing in stratified channel flow, *Proceedings 2nd International Symposium on Stratified Flows*, Trondheim, Norway, 1980.

[16] Rodi, W., *Turbulence Models and Their Applications in Hydraulics,* Book publication of International Association for Hydraulic Research, Delft, The Netherlands, 1980.

[17] Chu, V.H. and Baddour, R.E., Turbulent stratified shear flows, *J. Fluid Mechanics*, Vol. 132, 1984, pp. 353-378.

[18] Tan, L.W. and Chu, V.H., Lauber and Hager's dam-break wave data for numerical model validation, *J. Hydraulic Research*, Vol. 47(4), 2009, pp. 524-528.

[19] Tan, L.W. and Chu, V.H. Simulation of wave fronts on dry bed using Lagrangian blocks, *J. Engineering and Computational Mechanics*, Vol. 162(EM2), 2009, pp. 57-66.

[20] Tan, L.W. and Chu, V.H., Wave runup simulations using Lagrangian blocks on Eulerian mesh, *J. Hydro-Environ. Res.*, Vol. 3 (4), 2010, pp. 193-200.

[21] Tan, L.-W. and Chu, V.H., Two-dimensional simulation of shallow-water waves by Lagrangian block advection, *Computers and Fluids*, Vol. 65, 2012, pp. 35-43.